Active Thermography Data-Processing Algorithm for Nondestructive Testing of Materials

WELLINGTON FRANCISCO DA SILVA[1], RENAN A. C. MELO[1], MARCELLA GROSSO[2], GABRIELA R. PEREIRA[2], AND DOUGLAS BRESSAN RIFFEL [1]

[1]Department of Mechanical Engineering, Federal University of Sergipe, University City Prof. José Aloísio de Campos, São Cristóvão 49100-000, Brazil
[2]Non-Destructive Testing, Corrosion and Welding Laboratory, Federal University of Rio de Janeiro, Rio de Janeiro 21941-901, Brazil

Corresponding author: Douglas Bressan Riffel (dougbr@academico.ufs.br)

ABSTRACT This article presents the development of an active thermography algorithm capable of detecting defects in materials, based on the techniques of Thermographic Signal Reconstruction (TSR), Thermal Contrast (TC) and the physical principles of heat transfer. The results obtained from this algorithm are compared to the TSR technique and the raw thermogram obtained by stepped thermography inspection. Experimentally, a short thermal pulse is used and the surface temperature of the sample is monitored over time with an infrared camera. Due to the volume of data, the first step is data compression. Newton's law of cooling was used to store the normalized temperature data pixel-by-pixel over time and a compression ratio of 99% was obtained. The main contributions of the developed algorithm are: only four parameters for data compression and the concept of change in the direction of the heat flow to delimit the edges of the defects, where the borders are identified with a remarkable accuracy. Some well known image processing technique are also integrated to improve the thermal analysis: edge detection/interface between the sample and the image background; consolidation in a single image by aggregating the indicators referring to the concept of cooling/heating time constant, maximum thermal amplitude and contrast.

INDEX TERMS Active thermography, thermal analysis, infrared imaging, data compression, change detection algorithms, image processing.

I. INTRODUCTION

The increasing demand for industrial machines and products that are more resistant, have higher damage tolerance and that can be subjected to greater stress is remarkable. Monitoring and testing are fundamental aspects for industrial manufacturing, to prevent failures and increase reliability in these rapidly changing industrial conditions. Nondestructive testing (NDT), which inspects materials for discontinuities in characteristics without destroying the object under examination, has been widely applied, e.g., internal defect detection in various composite structures [1]–[3].

Thus, the search for non-destructive techniques and their development for monitoring, evaluating and ensuring the integrity of these materials has become an important task. There are successful applications of nondestructive testing and evaluation (NDT & E) techniques - such as eddy current, ultrasound, acoustic emission, X-ray and thermography - for damage detection in materials [4].

Infrared thermography (IRT) is used as a non-invasive monitoring technique in several industrial sectors and is effective for defects inspection in the microelectronic packaging industry. This technique has been used as a non-destructive technique in order to avoid unexpected equipment stops [5], [6]. IRT allows the operator to obtain a surface temperature map of any sample, regardless of the geometry, from the thermal energy radiated in the infrared electromagnetic band and from the heat flow [7]. Thermal cameras measure the apparent temperatures of each pixel, which include transmitted and reflected components that are considered noise.

The associate editor coordinating the review of this manuscript and approving it for publication was Xiaokang Yin.

The atmosphere itself can emit radiation owing to its temperature warm or hot objects in the surroundings (even the thermographer is a source) may lead to reflections of additional IR radiation from the object or windows. This fact makes this technique very accurate in measuring temperature variations, in both spatial and temporal ways. Thus, it is important to keep the environmental conditions constant during the test [8].

In non-destructive tests, the most used form of active thermography involving an external source of heat is flash thermography, also known as stepped thermography (PT). In PT, a heat step is applied to the surface of the sample and its thermal response is monitored during the cooling phase [9]–[11]. Different geometries, as well as internal discontinuities (e.g. voids, defects, corrosion), modify this thermal response and produce hot or cold areas on the sample surface sites. To improve the identification of defects, it is then necessary to automate the image processing [12].

Shepard [13] developed the methodology called Thermographic Signal Reconstruction (TSR), which involves data compression by way of curve fitting, usually a fifth to eighth degree polynomial, on a log-log scale (logarithmic in time and temperature). Compression occurs because it is only necessary to store the adjusted polynomial coefficients for each pixel in the image [14]. The first and second derivatives of the adjusted polynomials are then calculated. As a result, the images formed by the coefficients of the temperature polynomials in time, of the first and of the second derivative, are analyzed. Balageas *et al.* [15] and Shepard [16] showed that the TSR technique reduces temporal noise with the application of the logarithm, improves visual detection and allows the detection of defects in materials with low thermal conductivity.

The visibility of defects depends on several factors, including, for example, material characteristics, environmental conditions and equipment sensitivity. With regard to the material, both thermal properties (thermal conductivity, thermal diffusivity) and defects geometry are decisive.

In particular, the main interest of this research is to develop an algorithm for detecting defects in insulating materials using physical concepts of heat transfer. Our objectives include: compressing data with the use of curve fitting and characterization of the defects captured by the time constant; finding maximum contrast; determining ΔT_{max} of each pixel and maximum contrast (between the pixel and the maximum / minimum temperature of each frame); segmentation of regions of interest (defects), highlighting the background of the sample image; identification of the defects by the edges and understanding the physical meaning of the heat flow change, in order to reduce the subjectivity of the operator by obtaining a unique RGB image as a final result.

The paper is organized as follows: Section II discusses the description of the experiment and the methodology; Section III presents the algorithm development, and Section IV presents the results. Final comments and remarks are presented in Section V.
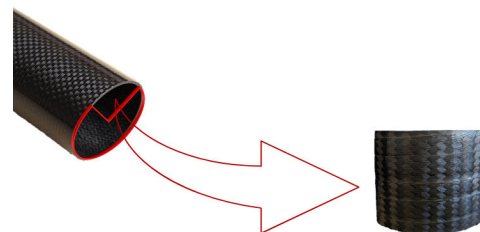

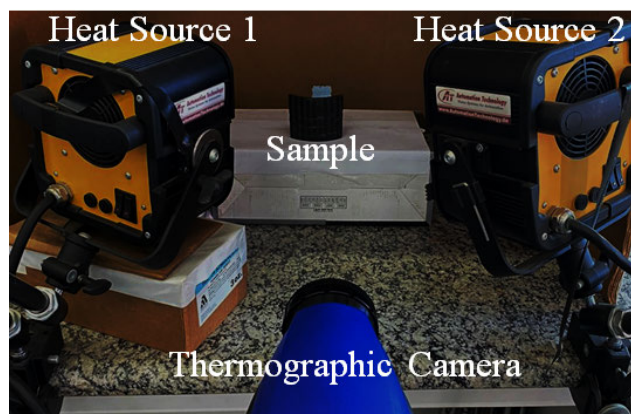**FIGURE 1.** Original pipe and sample with internal defects.

FIGURE 2. Experimental setup.

II. Description of the Experiment

Thermographic analysis was used to detect internal defects from images of an infrared camera that received radiation from a sample heated by a pulse and cooled down to the equilibrium temperature of the environment. A sequence of thermograms and the temperature distribution on the surface of the material over time were collected, allowing analysis of the thermal gradient in the material. As a case study for the algorithm, stepped thermography was applied to a carbon fiber reinforced polymer (CFRP) sample as shown in Fig. 2 . The main weakness of CFRP composite materials is their low impact resistance. Indeed, a visual and non-intrusive method that is able to detect impact damage with high efficiency and reliability is needed [17].

The sample was initially in the form of a pipe (5 mm thickness) made by manual lamination and vacuum compression. However, in order to carry out the tests, the circumference of the pipe was sectioned into four equal parts of 90°. In one of these parts, defects of different diameters and depths were caused to the inner surface of the sample, which are not observable by simple visual inspection from the outside. Tab. 1 shows the geometric specifications of each defect contained in the sample. The sample was extracted from an oil pipe, see Fig. 1

For the experimental test, a FLIR SC640 thermographic camera was used and the distance from the sample to the camera lens was 0.40 m. Because the modality to be evaluated in this study was active thermography, it was necessary to use an external source for thermal excitation. In this case, two halogen lamps, totaling 5.0 kW, were used as a thermal flash

TABLE 1. Geometric specification of defects.

	Fault 1	Fault 2	Fault 3	Fault 4
Diameter (mm) Hole	4.94	9.84	9.77	9.78
Depth (mm) Sample	4.38	4.55	2.35	4.24
thickness (mm)		5.6		

TABLE 2. Experimental conditions.

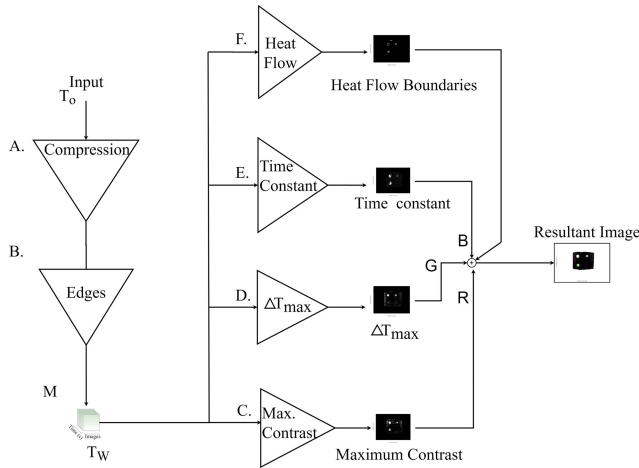| Emissivity (ϵ)	0.92	Initial temp. (K)	298.25
Total time (s)	60	Ambient temp. (K)	298.75
Heating time (s)	10	Humidity (%)	55

FIGURE 3. Algorithm Development.

source. Fig. 1 and Fig. 2 show the experimental setup, as well as one of the specimens. The test conditions were in accordance with specific standards. Data shown in Tab. 2 refers to the experimental conditions. An expert infrared technician conducted the experiment, according to the state of the art and following these standards: ASTM E1933-14 and ASTM E2582-19. The parameters are not optimized for the proposed algorithm and this could improve the results.

The experimental tests were carried out at the Laboratory of Non-Destructive Testing, Corrosion and Welding (LNDC) of the Federal University of Rio de Janeiro. The configuration of the samples can be seen in Tab. 1 and Tab. 2. In principle, any insulate material is suitable to be used.

III. ALGORITHM DEVELOPMENT
A flowchart of the algorithm is shown in Fig. 3. It starts with the compression of the data, which is a data adjustment (curve fitting) over time. Than, the edges of the sample are identified and the background is cropped. Three indicators are calculated to fill each channel of the RGB image and an unique image is built as result. The first indicator is the maximum contrast, the second is the ΔT_{max} of each pixel and the time constant is the last. The concept that the heat flow changes its direction at the boundary of the defects is used and added to the resulting image. It is expected to provide the operator with a simple and practical understanding of the
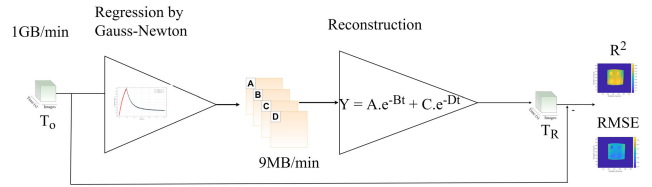

FIGURE 4. Flowchart of the compression procedure.
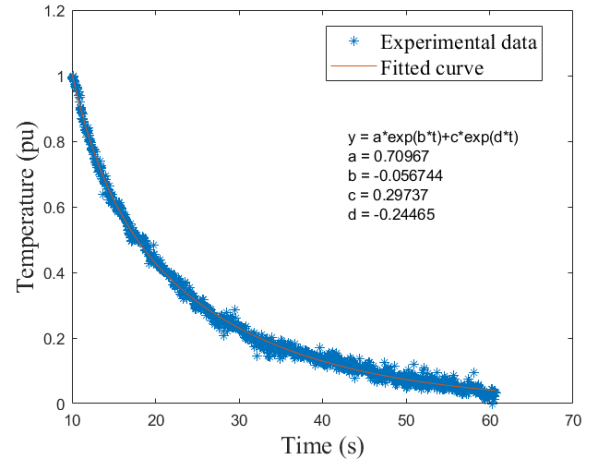

FIGURE 5. Curve fitting the cooling phase by the Gauss Newton Method.

physical concepts involved, what can be translated into agility in decision making by characterizing the defects

A. COMPRESSION
To understand the compression procedure, a flowchart is shown in Fig. 4. The radiometric images were extracted from a thermographic video and transformed into a matrix containing the temperatures for each of the pixels in space $T_0(x, y)$ at each time interval (e.g. $t = 1/30$ s).

The temperature signal from each pixel is normalized as displayed in Fig. 5, where the data and the curve adjusted by Eq. 1 fits the normalized signal through time. The pixel whose temperature signal is shown in Fig. 5 was arbitrarily chosen in a sample without defect, only to illustrate the method. The curve is fitted independently to both the cooling and heating phases.

$$y = a.e^{-b.t} + c.e^{-d.t}, \tag{1}$$

Among the coefficients, b and d are the inverses of the time constants. The Gauss-Newton method was used to fit the curves. However, before adjusting them, it is recommended to normalize the signal from each pixel and to apply median filters to eliminate some noise (high frequency) and to facilitate the adjustment, making the convergence faster.

In order to separate the phases, the maximum temperature of each pixel was obtained. These values and the frame where the maximums occur were stored. We proposed to store the heating phase because it could be used for future reference and to allow the original data to be excluded. The adjustment was achieved in a similar way to the cooling
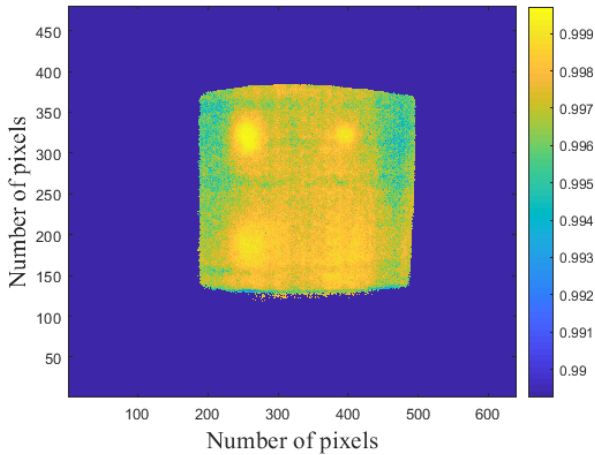
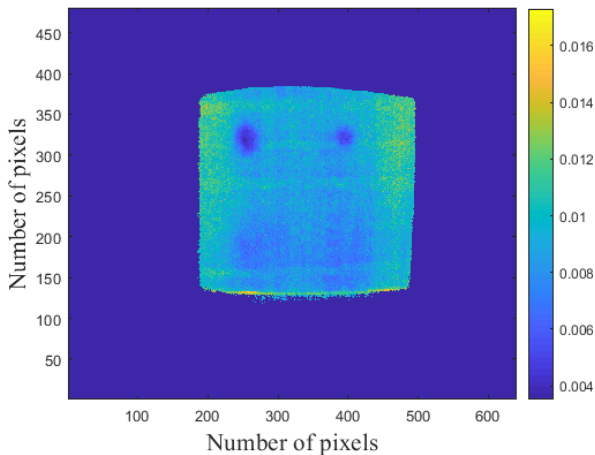**FIGURE 6.** Determination coefficient (R^2) of cooling phase.

FIGURE 7. Root Mean Square Error (RMSE) - cooling phase.

phase, i.e. through the sum of exponentials. However, this only requires one time constant, which means, from Eq. 1, that the value of d for the heating phase is equal to zero. Maps of the coefficient of determination (R^2) and root Mean Square Error (RMSE) are presented in Fig. 6 and Fig. 7 [18], [19], respectively. These indicate the quality of the data in each pixel.

Using this compression procedure, it was possible to reduce the temperature matrix from 800MB to 9MB - that is 98.88% of compression. To reconstruct the temperature matrix it was necessary to store the following sixteen matrices:

- Initial heating phase temperatures;
- Four matrices with the coefficients of the heating phase;
- R2 and RMSE correlation matrices of the heating phase;
- Maximum temperatures and their frames, marking the end of the heating and the beginning of the cooling phase;
- Four matrices with the coefficients of the cooling phase;
- R2 and RMSE correlation matrices of the cooling phase;
- Final temperatures.

Being in a noisy measurement, there is an expected error between the reconstructed temperature matrix (T_R) and the raw data (T_0).
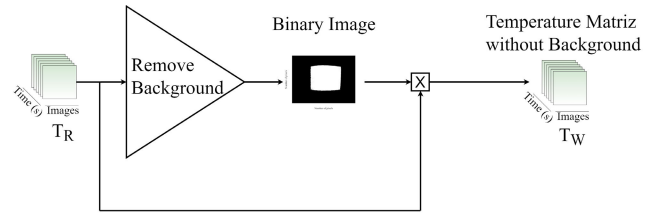

FIGURE 8. Flowchart of the sample detection procedure.

Another important point to consider is the physical meaning of the parameter adjustment because, unlike TSR where the polynomial adjustment is random, the model proposed here considers the restrictions of the physical phenomenon, hence following the laws of heat transfer and thermodynamics. It is possible to verify the similarity between Newton's Law of Cooling in Eq. 1 and the adjustment with the sum of the exponential model in Eq. 2:

$$T = T_a + (T_0 - T_a).e^{\frac{(t-t_0)}{\tau}}, \qquad (2)$$

where T is the system temperature, T_a is the ambient temperature, T_0 is the temperature at time $t = t_0$ and τ is the time constant.

B. EDGE DETECTION OF THE SAMPLE

Given a thermographic image, if the edges of the sample could be identified and the background cropped, it could reduce the matrix size and improve the image processing time. In the analysis process, segmentation is usually used to detect discontinuities and constant characteristics. Thresholding, region grouping, and edge detection are techniques used in segmentation [20]–[22].

Fig. 8 shows the flowchart of how this segmentation is done. The procedure consists of the following steps:

- First, a ΔT matrix is calculated, by subtracting the minimum from the maximum temperature for each pixel. Remember that both matrices are already available after the compression procedure (Subsection III-A);
- Subsequently, a linear transformation (local thresholding) is applied, which is basically the difference between the normalized ΔT matrix and the threshold (a value between 0 and 1). The value for this study case was 0.6. The result of this difference is a binary image;
- The product of this binary image and the temperature matrix results in a matrix of temperatures without background, where only the sample data is kept for analysis.

To illustrate the result (Fig. 9), Canny edge detector was applied in the binary image.

C. THERMAL CONTRAST

Thermal Contrast (TC) is the technique to find the maximum temperature difference between defective and non-defective regions [23]. In our algorithm, it is proposed to normalize the pixels independently. By applying this normalization and finding the minimal and maximal temperature in each frame, two curves are found (Fig. 10). Basically, they are two
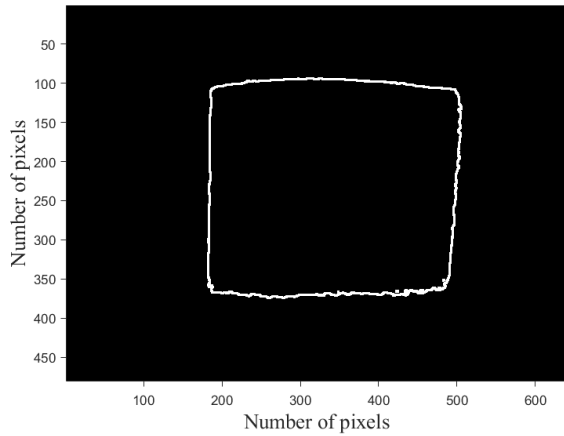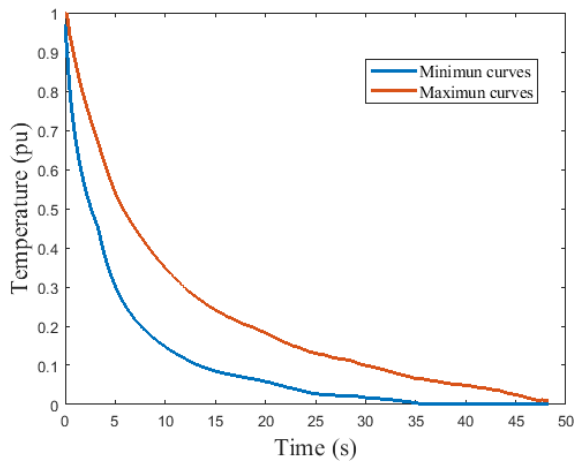
FIGURE 9. Detected edges of the sample.

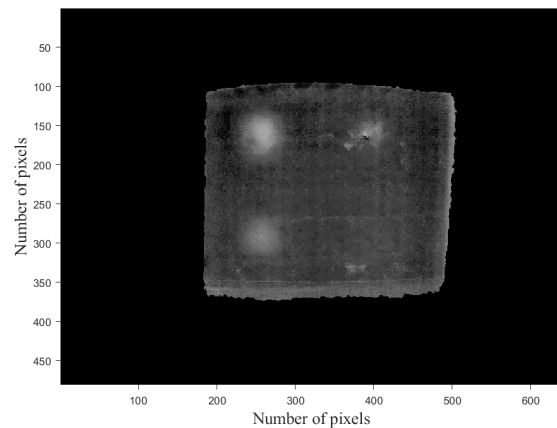**FIGURE 10.** Normalized maximum and minimum temperature curves.

FIGURE 11. Maximum thermal contrast using the minimum curve.

FIGURE 12. Maximum thermal contrast using the maximum curve.
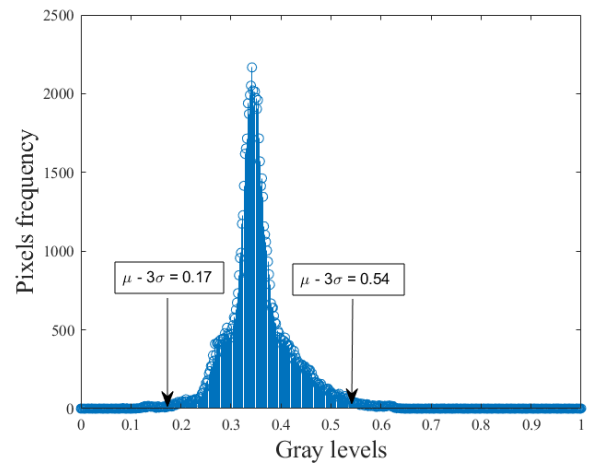
FIGURE 13. Histogram of the maximum contrast between the minimum curve variation and each pixel of the image with.

The image in Fig. 11 has the following histogram (Fig. 13), excluding the background zeros. Due to its similarity to a normal distribution, it was proposed to crop it in 99.87% pixels to enhance the contrast. The procedure computes the mean value of the entire matrix (μ) and the standard deviation (σ), cropping them at $\mu \pm 3\sigma$. As a result, the image in Fig. 14 shows the maximum thermal contrast using the minimal curve as reference, highlighting the contrast in the range ($\mu \pm 3\sigma$).

D. THERMAL AMPLITUDE

Another thermal indicator of a defect proposed for this algorithm is the difference between maximum and minimum temperature of each pixel. It was already used for sample detection (Subsection III-B). Fig. 15 shows this matrix, already cropped at ($\mu \pm 3\sigma$) to highlight the contrast. The result is quite accurate and it is very simple to implement.

E. TIME CONSTANT

Similar to the TSR technique, images can be generated with the coefficients from the fitted model (Eq. 1).

vectors: one with the maximal and the other with minimal temperature of the sample in each frame.

The next step is to find out the maximum thermal contrast by the difference between the minimum curve and each pixel of the image (Fig. 11). It is possible to evaluate the contrast using the maximum curve (Fig. 12), however, in this case, it results in a poor image and it was discarded.
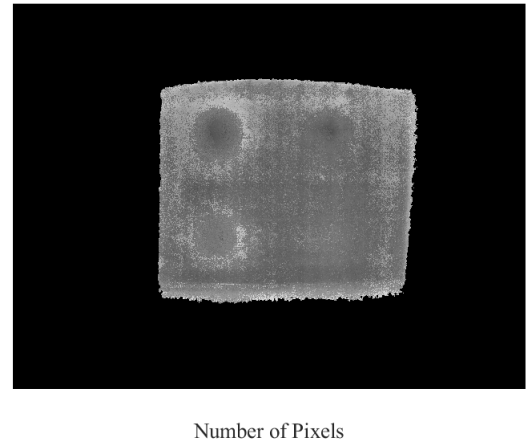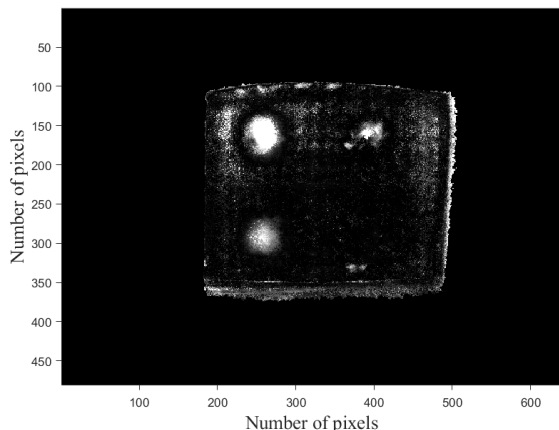
FIGURE 14. Maximum thermal contrast image cropped at ($\mu \pm 3\sigma$).
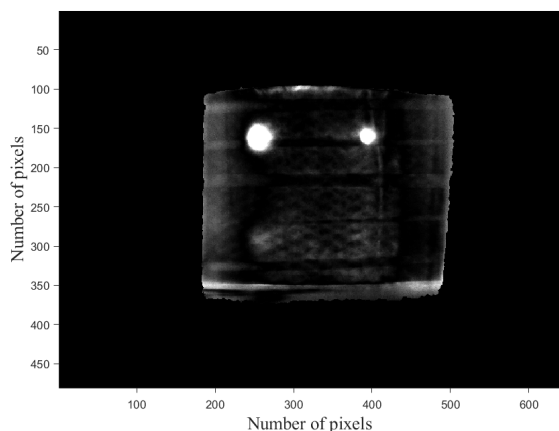

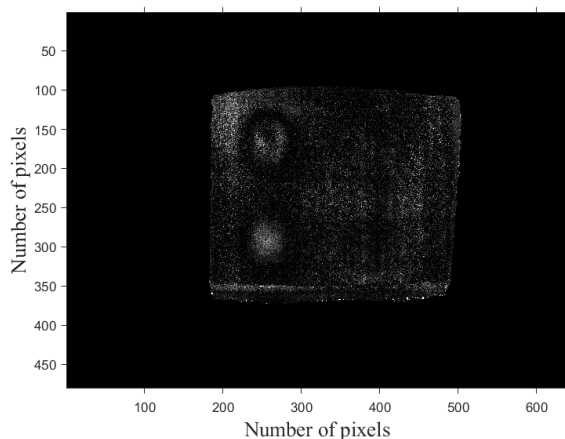**FIGURE 15.** Maximum Thermal Amplitude image cropped at ($\mu \pm 3\sigma$).

FIGURE 16. Time constant *B* in the cooling phase cropped at ($\mu \pm 3\sigma$).

By analyzing Fig. 16 and Fig. 17, it should be noted that the constant *D* is dominant, having an order of magnitude greater than seven times the constant *B*. Therefore, the matrix *D* is used. Another relevant factor is that the defects probably have a time constant greater or less than the surrounding region. These figures are also highlighting the contrast enhancement in the range ($\mu \pm 3\sigma$).
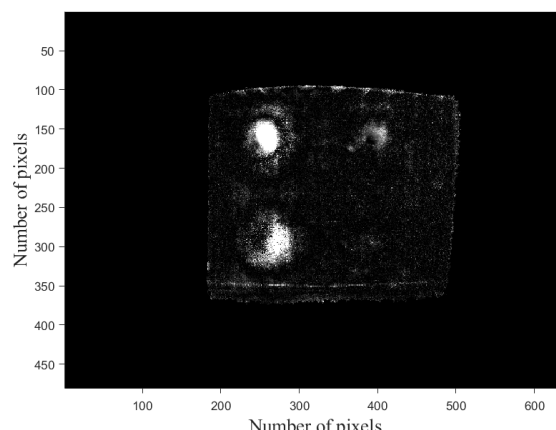

FIGURE 17. Time constant *D* in the cooling phase cropped at ($\mu \pm 3\sigma$).
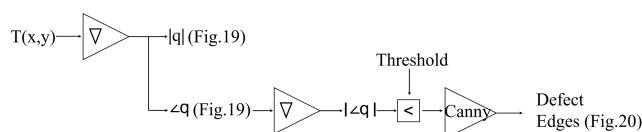

FIGURE 18. Heat flow algorithm for defect edge detection.

F. DEFECT EDGE DETECTION BY HEAT FLOW

In the literature, the use of heat flow for edge detection uses the concept of anisotropic heat diffusion, where the Laplacian of the temperature is used as indicator [24], [25]. In this algorithm, it is proposed to use the concept of heat conduction, where its flow is calculated by the Fourier's law:

$$q = -k.A.\nabla T = -k.A.\left[\frac{\partial T}{\partial x}, \frac{\partial T}{\partial y}\right]. \qquad (3)$$

where *k* is the thermal conductivity of the material and *A* is the section area. In this study, the gradient was solved by an approximate finite difference method without any correction of perspective or image distortion.

The proposed edge detector is based on the principle that the conduction heat flow changes its direction in discontinuities. This means that at the edges of the defects, heat flow should change its direction. This could reflect a geometry change in the contour region of the defect or any change in the composition or structure of the material. In our case, in which holes were made artificially (Tab. 1), a singularity happens at the edge, changing abruptly the area (*A*) and, consequently, the heat flow (*q*). Within the faulty region, the heat flow distribution should be more continuous, symmetrical, forming flow lines with a more uniform variation in a given direction. At the edges, however, abrupt alternations of direction characterize a diffuse region of heat flow. Fig. 19 shows the heat flow vectors of the sample. The sample and defects borders, together with a close up on Fault 02 were added only to illustrate the concept. The magnitudes are proportional to the sizes of the arrows and the inclinations show the heat flow angles.

Fig. 18 shows the flowchart of the calculus, where a gradient is computed in the temperature image, providing the
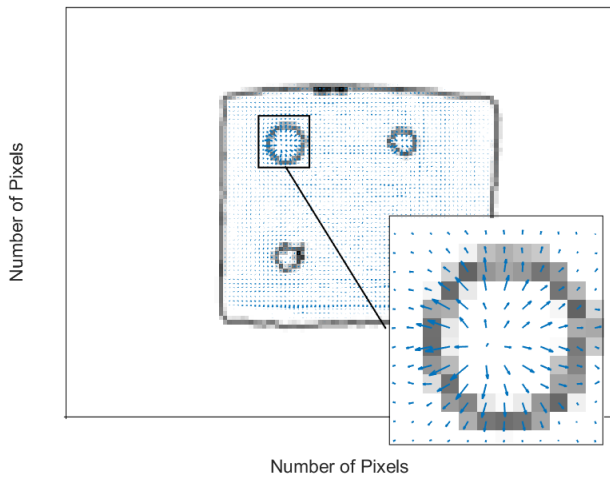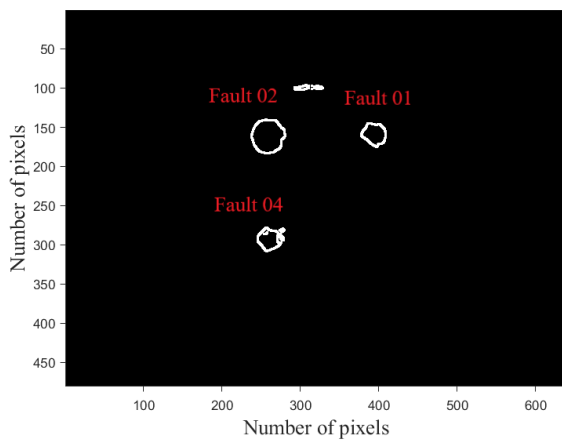
FIGURE 19. Heat flow and detail on Fault 02.

FIGURE 20. Detection of edge of the defects by the proposed algorithm.

FIGURE 21. Resultant image of the developed algorithm.
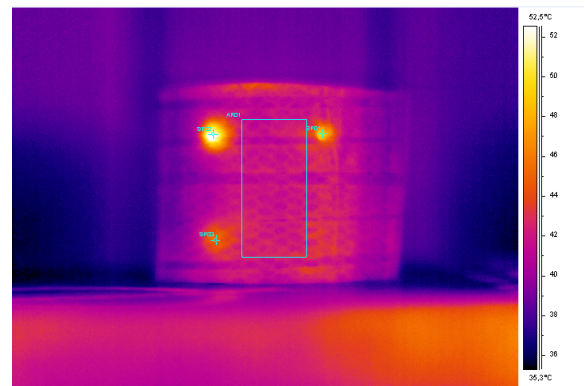
FIGURE 22. Best frame of thermal image without filter.
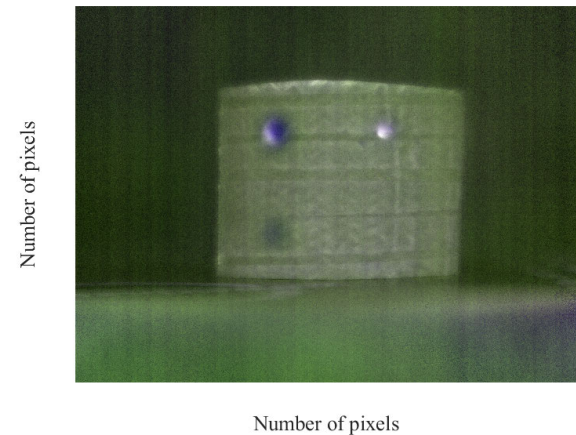
FIGURE 23. Resultant Image of the TSR technique with a octic polynomial.

modulus and the angle of the conduction heat flow in the image. Mathematically, the direction change of the heat flow is detected through the derivative of the angle. The derivatives are thresholded, thus generating a binary image to which a Canny edge detector is applied. Fig. 20 shows the output of the edge detection step.

IV. ALGORITHM RESULTS AND VALIDATION

The proposed algorithm combines all indicators in one RGB figure. Fig. 21 shows the output image of the algorithm. When all indicators converge in a certain area its color tends to white.

Two consolidated techniques were used as baselines for the same experiment: an advanced TSR technique and a thermogram

Thermograms are thermal images that display the amount of infrared energy emitted, transmitted, and reflected by an object. We used the FLIR®Atlas SDK for MATLAB® to convert the thermal video into temperature matrices. A skilled operator analysed the thermal video and chose the frame displayed in Fig. 22 as the best.

Roche *et al.* [26] proposed a method to create a unique RGB image using TSR and its result is compared with other techniques: Pulse Phase Thermography (PPT), Principal Component Thermography (PCT) and High-Order Statistics (HOS). The results show that the TSR composite image is the best. The same procedure described in that paper was applied here and the result is shown in Fig. 23. It is composed by the trio of coefficient images (5, 6 and 7) of the polynomial of degree 7, the same applied in the original paper.

Using the same criteria of comparison adopted in Roche *et al.* [26], the algorithm proposed in this paper has higher contrast, better sensitivity to the defect depths and lower noise. The resultant image is quite direct and clean, filtering even the fibers of the CFRP tube.

V. CONCLUSION

The developed algorithm was based on the physical concepts of heat transfer and took some ideas from: the Thermographic Signal Reconstruction (TSR) and Thermal Contrast (TC) techniques. The use of Newton's Cooling Law equation reaches almost 99% compression of the data. Comparing to the state of the art, the TSR technique normally uses more than seven parameters to compress the data. It takes the logarithm on both axes and then fits a polynomial, losing completely the physical meaning of the parameters. In the proposed compression method, each parameter maintains its meaning. A further innovation of the algorithm was the use of the concept of change in direction of the heat flow to delimit the edges of the defects, where the borders of the defects are plotted with a remarkable accuracy as shown in Fig. 20.

Other concepts such as the time constant of the heating and cooling phase, the concept of maximum thermal contrast and thermal amplitude were utilized. All these indicators were used to build an unique image. As described, before each indicator is inserted into the RGB channels, all data are normalized and cropped outside the range of ($\mu \pm 3\sigma$). This procedure computes the mean value of the entire matrix (μ) and the standard deviation (σ). The idea is take 99.87% of a normal distribution using the range 3σ and crop them at this limit.

To summarize, the main advantages provided by the algorithm are:

- Use of the concept of change in direction of the heat flow to delimit the edges of the regions of interest (where the defects are probably located). It is a new approach and results in Fig. 20, where the borders of the defects are plotted with a remarkable accuracy;
- Data compression: Newton's law of cooling was used as the basis of the phenomenon and a compression ratio of 99 % was obtained. It uses only 4 parameters as shown in Eq. 1, where the other techniques normally use more than 7 parameters;
- Compression of the heating phase data (which are neglected by the other techniques);
- Object segmentation between the sample and the image background;
- Indicator 1 (Red channel) which receives the maximum thermal contrast, as described in subsection III-C and shown in Fig. 14;
- Indicator 2 (Green channel) which corresponds to the maximum thermal amplitude (subsection III-D) as shown in Fig. 15;
- Indicator 3 (Blue channel) which receives the dominant time constant, as discussed in subsection III-E and illustrated in Fig. 17;

- Finally, the edges of the defects were added to the resulting image (Fig. 21), reducing the subjectivity of the operator and improving the effectiveness of this thermographic technique;
- One important advantage of the proposed algorithm, compared to the state of the art, is that it filters the fibers of the tube and highlights only the defects.

In addition to these advantages, the algorithm also has some limitations:

- It requires some adjustment by the operator - e.g., the local threshold;
- The quality of the radiometric videos influences the performance of the algorithm: for example, the ambient conditions and the characteristics of the heating process;
- It is more suitable for low conductivity materials.

Despite all the advantages presented and the good results obtained, the presented results show that the technique still needs future improvements, in order to automate the threshold adjustment and validate it for a wider range of materials and defects.

REFERENCES

[1] C. Meola, S. Boccardi, and G. M. Carlomagno, *Infrared Thermography in the Evaluation of Aerospace Composite Materials: Infrared Thermography to Composites*. Chicago, IL, USA: Woodhead, 2016.

[2] J.-Y. Wu, S. Sfarra, and Y. Yao, "Sparse principal component thermography for subsurface defect detection in composite products," *IEEE Trans. Ind. Informat.*, vol. 14, no. 12, pp. 5594–5600, Dec. 2018.

[3] R. Usamentiaga, Y. Mokhtari, C. Ibarra-Castanedo, M. Klein, M. Genest, and X. Maldague, "Automated dynamic inspection using active infrared thermography," *IEEE Trans. Ind. Informat.*, vol. 14, no. 12, pp. 5648–5657, Dec. 2018.

[4] S. E. Burrows, A. Rashed, D. P. Almond, and S. Dixon, "Combined laser spot imaging thermography and ultrasonic measurements for crack detection," *Nondestruct. Test. Eval.*, vol. 22, nos. 2–3, pp. 217–227, Jun. 2007.

[5] S. Bagavathiappan, B. B. Lahiri, T. Saravanan, J. Philip, and T. Jayakumar, "Infrared thermography for condition monitoring—A review," *Inf. Phys. Technol.*, vol. 60, pp. 35–55, Sep. 2013.

[6] M. Grosso, J. E. C. Lopez, V. M. A. Silva, S. D. Soares, J. M. A. Rebello, and G. R. Pereira, "Pulsed thermography inspection of adhesive composite joints: Computational simulation model and experimental validation," *Compos. B, Eng.*, vol. 106, pp. 1–9, Dec. 2016.

[7] F. J. Madruga, C. Ibarra-Castanedo, O. M. Conde, J. M. López-Higuera, and X. Maldague, "Infrared thermography processing based on higher-order statistics," *NDT Int.*, vol. 43, no. 8, pp. 661–666, Nov. 2010.

[8] S. D. Holland and R. S. Reusser, "Material evaluation by infrared thermography," *Annu. Rev. Mater. Res.*, vol. 46, pp. 287–303, 2016.

[9] M. P. Connolly, "A review of factors influencing defect detection in infrared thermography: Applications to coated materials," *J. Nondestruct. Eval.*, vol. 10, no. 3, pp. 89–96, Sep. 1991.

[10] M. Grosso, I. de Araájo Soares, J. E. C. Lopez, S. D. Soares, J. M. A. Rebello, and G. R. Pereira, "Study on the limit detection of defects by pulsed thermography in adhesive composite joints through computational simulation," *Compos. B, Eng.*, vol. 168, pp. 589–596, Jul. 2019.

[11] G. Inglese, R. Olmi, and S. Priori, "A procedure for detecting hidden surface defects in a thin plate by means of active thermography," *J. Nondestruct. Eval.*, vol. 36, no. 3, p. 61, Sep. 2017.

[12] P. Zhu, L. Tian, and Y. Cheng, "Improvement of defect feature extraction in eddy current pulsed thermography," *IEEE Access*, vol. 7, pp. 48288–48294, 2019.

[13] S. M. Shepard, "Temporal noise reduction, compression and analysis of thermographic image data sequences," U.S. Patent 6 516 084, Feb. 4, 2003.

[14] S. M. Shepard, "Advances in pulsed thermography," *Proc. SPIE*, vol. 4360, pp. 511–516, Mar. 2001.

[15] D. Balageas, B. Chapuis, G. Deban, and F. Passilly, "Improvement of the detection of defects by pulse thermography thanks to the TSR approach in the case of a smart composite repair patch," *Quant. Infr. Thermography J.*, vol. 7, no. 2, pp. 167–187, Dec. 2010.

[16] S. M. Shepard, "Flash thermography of aerospace composites," in *Proc. Conf. Panamericana Buenos Aires*, vol. 7, 2007, pp. 1–10.

[17] Y. Li, A. B. Ming, H. Mao, G. F. Jin, Z. W. Yang, W. Zhang, and S. Q. Wu, "Detection and characterization of mechanical impact damage within multi-layer carbon fiber reinforced polymer (cfrp) laminate using passive thermography," *IEEE Access*, vol. 7, pp. 27689–27698, 2019.

[18] D. Palumbo, P. Cavallo, and U. Galietti, "An investigation of the stepped thermography technique for defects evaluation in GFRP materials," *NDT Int.*, vol. 102, pp. 254–263, Mar. 2019.

[19] H. Zhao, Z. Zhou, J. Fan, G. Li, and G. Sun, "Step-heating infrared thermographic inspection of steel structures by applying least-squares regression," *Appl. Opt.*, vol. 56, no. 4, pp. 1238–1245, 2017.

[20] S. Sfarra, C. Ibarra-Castanedo, C. Santulli, D. Paoletti, and X. Maldague, "Monitoring of jute/hemp fiber hybrid laminates by nondestructive testing techniques," *Sci. Eng. Composite Mater.*, vol. 23, no. 3, pp. 283–300, May 2016.

[21] W. E. Snyder and H. Qi, *Machine Vision*. Cambridge, U.K.: Cambridge Univ. Press, 2010.

[22] P. Soille, *Morphological Image Analysis: Principles Application*. Cham, Switzerland: Springer, 2013.

[23] S. K. Lau, D. P. Almond, P. M. Patel, J. Corbett, and M. B. Quigley, "Analysis of transient thermal inspection," in *Infrared Technology and Applications*, vol. 1320, A. H. Lettington, Ed. Oct. 1990, pp. 178–185. [Online]. Available: http://proceedings.spiedigitallibrary.org/proceeding.aspx?doi=10.1117/12.22325

[24] P. Perona and J. Malik, "Scale-space and edge detection using anisotropic diffusion," *IEEE Trans. Pattern Anal. Mach. Intell.*, vol. 12, no. 7, pp. 629–639, Jul. 1990. [Online]. Available: http://ieeexplore.ieee.org/document/149593/

[25] C. Direkoálu and M. S. Nixon, "Moving-edge detection via heat flow analogy," *Pattern Recognit. Lett.*, vol. 32, no. 2, pp. 270–279, Jan. 2011.

[26] J. M. Roche, F. H. Leroy, and D. L. Balageas, "Images of thermographic signal reconstruction coefficients: A simple way for rapid and efficient detection of discontinuities," *Mater. Eval.*, vol. 72, no. 1, pp. 73–82, 2014.
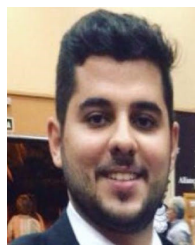
RENAN A. C. MELO was born in Aracaju, Brazil. He received the bachelor's degree in mechanical engineering from the Federal University of Sergipe, in 2019.

MARCELLA GROSSO received the bachelor's and M.Sc. degrees in metallurgical and materials engineering from the Federal University of Rio de Janeiro (COPPE/UFRJ), in 2016. She is currently pursuing the Ph.D. degree in nondestructive testing. She is also working with the Non-Destructive Testing, Corrosion and Welding Laboratory, COPPE/UFRJ.

GABRIELA R. PEREIRA received the degree in physics from the Federal University of Rio de Janeiro (UFRJ), and the master's and Ph.D. degrees in nuclear engineering from UFRJ, in 2010. She is currently a Leader with the Non-Destructive Testing, Corrosion and Welding Laboratory, COPPE/UFRJ. She has experience in Nuclear Engineering, acting on the following subjects: x-ray fluorescence, microtomography, synchrotron radiation, breast tissue, and lean duplex stainless steel.

WELLINGTON FRANCISCO DA SILVA was born in Jaboatão dos Guararapes, Brazil. He received the degree in electrical engineering from Faculty Pio Décimo, Aracaju, Brazil, the master's degree in electrical engineering from the Federal University of Sergipe (UFS), with his thesis on development of an algorithm for processing radiometric data obtained by pulsed active thermography, in 2019, the postgraduate degree in mineral technology from Federal University of Pará (UFPA) and in maintenance engineering from University of Rio Grande do Sul (PUC-RS), and the full degree in electromechanics from Federal Institute of Science and Technology Education of Minas Gerais (IFMG). He took a technical course in mechanics at the Federal Institute of Education, Science and Technology of Pernambuco (IFPE), Recife, Brazil. He worked as engineer at the Salobo and Sossego project, Mining Company Vale's largest copper operation, Canaã dos Carajás and Marabá, from 2003 to 2009, and Mining Paragominas, Brazil, from 2003 to 2009. He was a mechanical technician at Mining Company Vale's in potash mine in Taquari/Vassouras, Sergipe, Brazil, from 1997 to 2003. He has experience in the area of asset management with the implementation of Key Performance Indicators (KPIs) and the Fundamentals of Routine Program. He also has experience in contracts management and elaboration of equipment specifications, and failure analysis and reliability analysis. He currently participates in the energy research group in the field of solar energy at UFS with Prof. Douglas Riffel.

DOUGLAS BRESSAN RIFFEL was born in Curitiba, Brazil. He received the bachelor's degree in electrical engineering from the Federal Technological University of Paraná (UTFPR), the master's degree in electrical engineering from the Federal University of Ceará (UFC) with thesis on power electronics, and the Ph.D. degree in mechanical engineering from the Federal University of Paraíba (UFPB) with thesis on dynamics of adsorption chillers. The Ph.D. research was partially done (one year) at the Fraunhofer Institute for Solar Energy Systems (ISE), Freiburg, Germany. He is currently an Assistant Professor with the Federal University of Sergipe (UFS), Aracaju, Brazil. He has experience in Electric and Mechanical Engineering, with focus in electromechanical driven systems, solar energy conversion, inverse problems, and multi-objective optimization.

● ● ●